Facile Anhydrous Proton Transport on Hydroxyl Functionalized Graphane

Abhishek Bagusetty, Pabitra Choudhury, Wissam A. Saidi, Bridget Derksen, Elizabeth Gatto, and J. Karl Johnson

Phys. Rev. Lett. **118**, 186101 — Published 3 May 2017

DOI: 10.1103/PhysRevLett.118.186101

Facile Anhydrous Proton Transport on Hydroxyl Functionalized Graphane

Abhishek Bagusetty,[1,2,*] Pabitra Choudhury,[3,*] Wisssam A. Saidi,[4] Bridget Derksen,[2] Elizabeth Gatto,[2] and J. Karl Johnson[2,†]

[1] *Computational Modeling & Simulation Program, University of Pittsburgh, Pittsburgh PA 15260, USA*
[2] *Department of Chemical & Petroleum Engineering, University of Pittsburgh, Pittsburgh PA 15261, USA*
[3] *New Mexico Tech, Department of Chemical Engineering, Socorro NM 87801, USA*
[4] *Department of Mechanical & Materials Science, University of Pittsburgh, Pittsburgh PA 15261, USA*

(Dated: March 29, 2017)

Graphane functionalized with hydroxyl groups is shown to rapidly conduct protons under anhydrous conditions through a contiguous network of hydrogen bonds. Density functional theory calculations predict remarkably low barriers to diffusion of protons along a 1-D chain of surface hydroxyls. Diffusion is controlled by local rotation of hydroxyl groups, a mechanism that is very different from that found in 1-D water wires in confined nanopores or in bulk water. The proton mean square displacement in the 1-D chain was observed to follow Fickian diffusion, rather than the expected single-file mobility. Charge analysis reveals that the charge on the proton is essentially equally shared by all hydrogens bound to oxygens, effectively delocalizing the proton.

Transport of protons through membranes is of vital importance across a broad range of processes, ranging from biological systems to industrially-important technologies. We here report the first principles design of a novel material capable of facile conduction of protons in the complete absence of water, which addresses a critical challenge related to proton exchange membrane (PEM) fuel cells [1]. The most widely used PEM materials are polyelectrolyte polymers, such as Nafion [2]. These polymers conduct protons at appreciable rates only when hydrated. As a result, the upper limit for the operating temperature of PEM fuel cells is typically about 80°C because higher temperatures result in dehydration of the polyelectrolyte polymer [3], which causes a dramatic decrease in the rate of proton conduction. We show that functionalized graphane can conduct protons anhydrously at elevated temperatures, making it a potential material for intermediate temperature PEM fuel cells. There are several advantages to operating PEM fuel cells at intermediate temperatures (100–200°C), including increased electrochemical reaction rates, the availability of higher quality waste heat, and decreased CO poisoning of the anode [4]. Hence, there is a practical need for anhydrous proton transport (PT) membrane materials that has motivated research in this area [5].

A key requirement for a material to exhibit fast PT is optimal donor-acceptor spacing. Thus, facile anhydrous PT should occur on a surface having a fixed contiguous network of hydrogen bonded hydroxyl (OH) groups. Accordingly, we have used density functional theory (DFT) calculations to show that graphane (fully hydrogenated graphene) functionalized with hydroxyl groups has inherent near-optimal spacing for forming a surface network of hydrogen bonds capable of facilitating fast anhydrous PT. We show that this novel material offers both the opportunity for fundamental studies of anhydrous PT and the potential for creating new practical PEM membrane materials. The mechanism of PT in aqueous systems has been extensively studied and is well understood. In contrast, the PT mechanisms under anhydrous conditions appear to depend on the material and are a matter of debate [5–8]. This work provides atomic-level insight into how PT takes place on OH-functionalized graphane and why the barriers to PT on this material are so low.

Why Graphane? There are at least two advantages for use of graphane instead of graphene as the platform for constructing PT membranes: (1) proton exchange membranes must be electronic insulators and graphene is a semimetal, whereas hydroxylated graphane is an insulator with a direct band gap of 3.22 eV [9]; (2) graphane has sp^3 structure, whereas functionalized graphene has both sp^2 and local sp^3 structures, resulting in more strain compared with functionalized graphane. In addition, hydroxylated graphane is predicted to be stable [9]. Our model system is shown in Fig. 1 and consists of a periodic supercell of graphane having a one-dimensional (1-D) chain of OH groups spanning the cell. This system contains 4 OH groups and a single proton; the system has a +1e total charge. The hydroxyl groups can rotate about the C–O bonds and our relaxed structures show that these OH groups spontaneously orient to form a 1-D chain of hydrogen bonds as a result of the inherent structure of graphane, i.e., the natural distance of OH groups on graphane is nearly ideal for hydrogen bonding, with O–O distances of about 2.3 to 2.4 Å.

Calculation Method. We carried out DFT calculations using the Vienna *Ab-initio* Simulation Package (VASP) [18] and an in-house modified version of Quantum Espresso (QE) [19]. An energy cutoff of 520 eV was used with the Perdew-Burke-Ernzerhof form of the

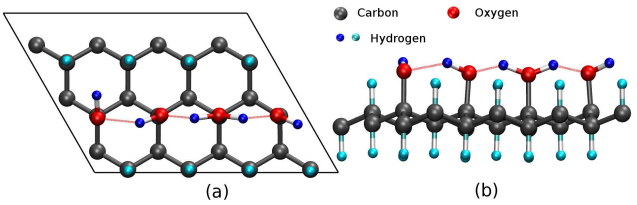

FIG. 1. (Color online) (a) Top view of the hydroxylated graphane supercell containing 24 carbons and 4 hydroxyl groups with one excess proton (carbons in gray, oxygens in red, hydrogens bound to oxygens in dark blue, hydrogens bound to carbon in light blue, red lines indicate hydrogen bonding). (b) Side-on view for the configuration in (a). Supercell lattice parameters are given in Table S1 of the Supplemental Material [10]. Solid lines show the cell boundaries in the a and b directions.

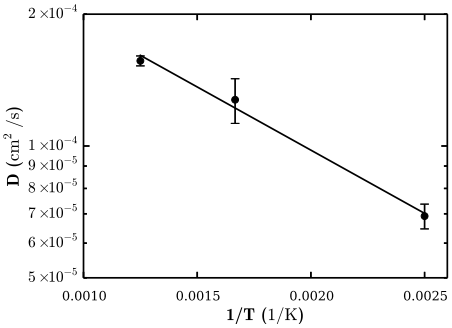

FIG. 2. Self-diffusion coefficients at temperatures of 400, 600, and 800 K as determined from AIMD simulations.

generalized gradient approximation [20]. We checked the convergence of the k-point grid and vacuum spacing to validate our computational setup. The minimum energy pathway (MEP) for PT was obtained using the climbing image nudged elastic band (cNEB) method [21]. The size of the supercell in the direction perpendicular to the graphane plane was 20 Å, ensuring interactions between the layers were negligible. Proton diffusivities were computed from Born-Oppenheimer *ab-initio* molecular dynamics (AIMD) simulations in the *NVE* (microcanonical) ensemble with a step size of 0.25 fs. Details are given in Supplemental Material [10].

Proton Transport Dynamics. The self-diffusion coefficients, D, at different temperatures are plotted in Fig. 2. Extrapolation of the data gives an estimate of D at room temperature of 4×10^{-5} cm^2s^{-1}, which is fortuitously close to the self-diffusion coefficient of protons through bulk water computed from molecular simulations [22]. Diffusion coefficients of protons through Nafion depend dramatically on the hydration level. Simulations predict that diffusivity increases from 1.4×10^{-6} to 1.7×10^{-5} cm^2s^{-1} at room temperature as the number of water molecules increases from 6 to 15 per sulfonic acid group [23]. These simulations are in good agreement with experimental measurements for Nafion under similar conditions [24]. Our data were fitted to an Arrhenius expression, which yielded an activation energy of 60 meV. This is significantly lower than the experimentally measured activation energy for proton conductance in Nafion, which ranges from 0.1 to 0.36 eV, depending on water content [25]. Analysis of the AIMD simulations indicated that proton hopping takes place in concert with the rotation of hydroxyl groups and this rotation is expected to be the rate limiting step in PT.

Proton Transport Energetics. The rate limiting step was confirmed by computing the MEP for PT from the cNEB method. Our calculated barrier height for proton hopping along the OH chain is about 70 meV, as shown in Fig. 3. This barrier height is in very good agreement with the activation energy of 60 meV estimated from AIMD diffusivity calculations. We note that exact agreement is not expected between barrier heights from cNEB and apparent activation energies from Arrhenius plots for several reasons: (1) the barrier heights from cNEB calculations are zero Kelvin electronic energies while activation energies are temperature-averaged Gibbs free energies, (2) the AIMD calculations include anharmonic effects that are not captured in the cNEB calculations, and (3) the diffusivities are subject to statistical errors. The very low barrier computed from cNEB (Fig. 3) provides a second confirmation (with the AIMD results) of our expectation that hydroxylated graphane will conduct protons at fast rates under anhydrous conditions. As we tentatively observed in the AIMD simulations, cNEB confirms that the PT pathway consists of a concerted hopping mechanism involving rotation of hydroxyl groups about the C–O bond axis, along with the displacement of a proton. Key configurations from the MEP are shown in Fig. 4. We note an unexpected feature in the MEP that is elucidated by examining the configurations in Fig. 4: the MEP has two transition states, separated by a very shallow local minimum metastable state. The two end-point geometries, (a) and (e) in Fig. 4, are identical by translational symmetry and are characterized by a single OH bond pointing perpendicular to the 1-D chain of OH groups, with the H atom pointing to the center of a hexagon in the underlying graphane. The metastable intermediate, Fig. 4 (c), is similar in structure, except that the OH group perpendicular to the chain is oriented over a graphane C–C bond. The two transition states are almost isoenergetic (Fig. 3) and are visually identical, as seen in Fig. 4 (b) and (d). The transition states correspond to an OH group just before and just after the C–C bond center crossing. We also note two distinct proton hopping events in Fig. 4, as defined by a change in the nearest O for a given H. We have ignored quantum diffraction effects in our calculations. Zero-point energy corrections obtained from vibrational frequency calculations reduce the classical barrier height from 70 to 40 meV. We have estimated rate constants for PT using three different transi-

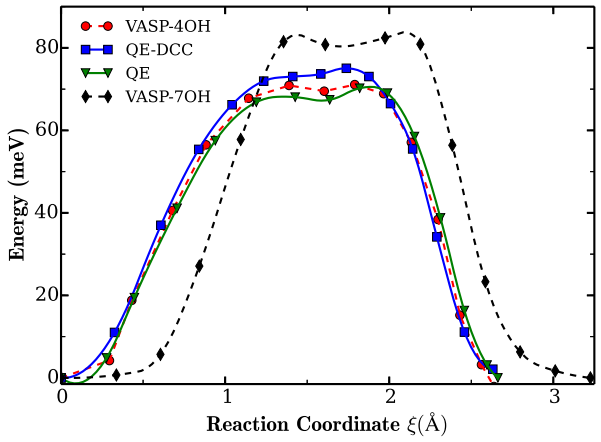

FIG. 3. (Color online) Minimum energy pathway (MEP) computed from the cNEB method for proton hopping on a 4-OH group system (see Fig. 1) computed from VASP (red circles) and Quantum Espresso (QE) without (green triangles) and with (blue squares) density-countercharge corrections. The MEP for a 7-OH group system is also shown (black diamonds) as a test of finite system size effects.

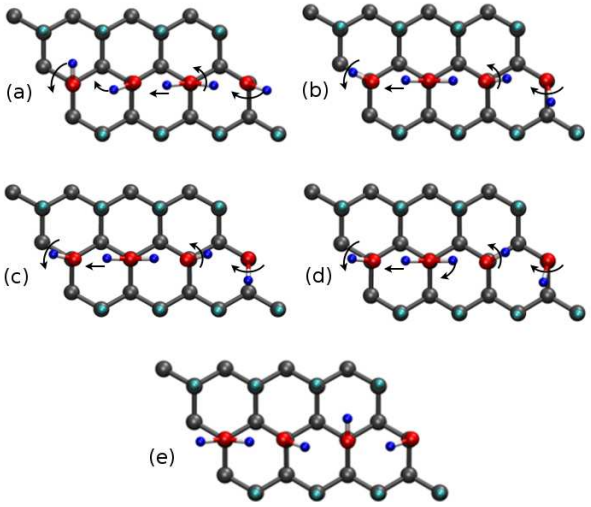

FIG. 4. (Color online) Atomic configurations computed from cNEB for the 4-OH group system (Fig. 1) for the (a) initial, (b) first transition state, (c) metastable intermediate, (d) second transition state, and (e) final state. The concerted motion in each step is indicated with arrows (colors defined in Fig. 1).

tion state theory (TST) approximations. Rate constants were determined using classical and quasi-classical treatment of TST [26], and tunneling effects were estimated using the semi-classical TST approximation [27]. Results from these calculations are shown in Fig. S1 of the Supplemental Material [10]. Tunneling effects were found to be negligible for the temperatures considered here. This is not unexpected because the proton hopping barrier is both small and broad (Fig. 3). On the other hand, quantum effects estimated from zero-point energy corrections through the quasi-classical TST approximation increase the rate constant by about a factor of 1.7 near room temperature. Therefore, our classical treatment can be viewed as a lower bound estimate to the diffusivity.

Interestingly, although there is formally only one proton in the system, each of the H atoms involved in hydrogen bonding behave essentially as protons, i.e., each H atom bound to an O atom can potentially hop. Moreover, the effective charges on the H atoms, as computed from the DDEC6 population analysis method [28], are almost identical (Table. S2, Supplemental Material [10]. Thus, the H atoms are, in a sense, indistinguishable, and the proton is highly delocalized. The charge delocalization is an unexpected feature and so we have verified that this is not an artifact due to system size effects by using a larger super cell; we also eliminated the possibility that the charge delocalization was due to self-interaction error by computing charges from Hartree-Fock level of theory (see Table S3 & S4, Supplemental Material [10]). Charge delocalization decreases the barrier to PT by reducing the polarization associated with moving a proton from one O atom to another.

We have estimated finite-size effects in our calculations by constructing a supercell consisting of 70 C atoms, 7 OH groups, and a single proton. Note that this system has different symmetry than the 4 OH system because of the odd number of OH groups in the unit cell. We have computed the cNEB MEP in this 7 OH system and plotted the results in Fig. 3. The MEP for the larger system has the same features as the smaller system and a barrier that is about 12 meV higher. The one qualitative difference between the two systems is that the 7 OH system has only a single proton hop (see Fig. S2 of the Supplemental Material [10]). This difference can be attributed to finite-size effects because rotation of an OH group in the smaller system has a larger influence due to periodic boundary conditions. Note also in Fig. 3 that the reaction coordinate ξ is somewhat larger for the 7 OH system, because of the larger number of moving atoms.

Challenges in charged systems. Periodic DFT calculations of charged systems are problematic because of errors due to imposing an artificial jellium background [29]. We have estimated the extent of this error by implementing the density-countercharge (DCC) method of Dabo et al. [30] in an in-house modified version of QE. We computed the cNEB pathways for the 4 OH system using both the original QE code (no DCC) and the DCC corrected code. These MEPs are plotted in Fig. 3. Adding the DCC corrections increases the barrier by about 5 meV, indicating that the errors introduced due to the jellium background are very small. We also note that the 7 OH system provides an independent check of the error due to the charge because the system is larger but has the same net charge. However, in this case, the difference between the two systems includes other effects due to flexibility and periodicity, in addition to the charge

density.

Transport mechanism details. One might assume that PT in the 1-D systems studied here would result in single-file mobility because the protons cannot pass one another. Single-file mobility is characterized by the mean square displacement (MSD) of protons being proportional to $t^{1/2}$, where t is time [31]. However, we found that this system follows the Einstein relation for Fickian diffusion (MSD $\propto t$) [31], as seen in Fig. S4 of the Supplemental Material [10]. We constructed a lattice model to test whether the Fickian diffusion observed from AIMD simulations was due to artifacts of system size or short simulation times. The results of the lattice model also show Fickian diffusion (see Fig. S4). The system with a single proton effectively behaves as being in the infinite dilution limit even though all of the hydrogens on OH groups can hop. This unexpected outcome can be rationalized by considering the case without a proton. In this case, one has a contiguous chain of hydrogen bonded OH groups, but no protons and therefore no PT can take place. Thus, the 1-D system is analogous to a 1-D lattice model, where the OH chain without a proton is like an empty lattice, the chain with a single proton is similar to a lattice with one occupied site, but having the unique feature that any of the H atoms on the chain can hop. Simulations of a lattice model with 8000 OH groups and 4000 protons show that this "half-filled" system exhibits the expected single-file mobility, with the MSD $\propto t^{1/2}$ (see Fig. S5, Supplemental Material [10]). Note that system size effects can give rise to anomalously large diffusivities for diffusion of fluids through very smooth nanopores [32, 33]. The hallmarks of this system size artifact are: (1) calculated diffusion barriers that are inconsistently large compared with measured diffusivities and (2) systematic deviations from MSD $\propto t$ [32]. Our system does not display anomalous diffusivities because the calculated diffusion barrier from cNEB is consistent with the barrier computed from AIMD (Figs. 2 and 3) and we clearly observe MSD $\propto t$ (Fig. S4).

Discussion. Several observations can be made based on our results. Firstly, the PT mechanism identified here is significantly different from mechanisms in bulk water and 1-D water wires. It has been shown that concerted PT through a Grotthuss mechanism [34] in both bulk water and water wires confined to 1-D channels, such as carbon nanotubes [35], results in unfavorable polarization of the water chain, the resolution of which requires significant solvent reorganization [8, 36]. Hydroxylated graphane has no hydrogen bonding defects like orientational D or L configurations as reported for PT in carbon nanotubes [36, 37], and hence there is no need for solvent reorganization. The only reorganization required is local in nature–involving the concerted rotation of a pair of adjacent OH groups. Moreover, since this system is anhydrous there is no large electrostatic penalty for desolvation, and the conductance of protons should not decrease with length of the 1-D path, as with narrow carbon nanotubes [35].

A second observation is that hydroxylated graphane is potentially a significantly better material for anhydrous proton exchange membranes than existing materials. Proton conduction on OH functionalized polymers [5, 38], ionic crystals [39], and doped amorphous carbons [40] has been demonstrated, but none of these materials have optimal placement of hydrogen bonding groups. Hence, they lack the contiguous network of hydrogen bonds required for truly facile water-free PT. As noted by Nagamani et al., the presence of a hydrogen bond network is vital to fast and robust PT [38]. Another advantage of a functionalized surface over polymers is the reduced flexibility of the surface relative to a polymer; flexibility in the polymer chain disrupts hydrogen bonds and decreases the PT rate.

It is interesting to note the similarities between the contiguous 1-D OH chain of Fig. 4 and the hypothetical soliton system studied previously [41]. Although the charge is highly delocalized, our system does not exhibit soliton-like collective PT. This is because proton transport coupled with rotation of an OH group is inconsistent with the soliton mechanism [41].

Hydroxylated graphane could potentially be produced by using electron-beam generated plasmas, which have been used to functionalize graphene with F, H, and O atoms [42]. This approach would produce a high degree of hydroxylation, rather than a 1-D chain of OH groups, but having a 2-D network of hydrogen bonds will provide redundant pathways for PT and thus be more robust than the 1-D system we have studied here. A single missing OH group in a 1-D chain effectively blocks PT (the estimated barrier is about 4.4 eV, see Fig. S9 and the discussion in the Supplemental Material [10]), so for any practical material, a 2-D network is desired. We are currently investigating the characteristics of PT in a 2-D network.

We thank G. Ciccotti and M. E. Tuckerman for helpful discussions. This work used the Extreme Science and Engineering Discovery Environment (XSEDE), which is supported by National Science Foundation grant number ACI-1053575, under allocation number TG-DMR110091. Calculations were also carried out at the University of Pittsburgh's Center for Research Computing. A.B. acknowledges graduate fellowship from Pittsburgh Quantum Institute.

* These authors contributed equally to this work.
† karlj@pitt.edu

[1] K. Kreuer, Chem. Mater. **8**, 610 (1996).
[2] V. Mehta and J. S. Cooper, J. Power Sources **114**, 32 (2003).
[3] M. A. Hickner, H. Ghassemi, Y. S. Kim, B. R. Einsla, and J. E. McGrath, Chem. Rev. **104**, 4587 (2004).
[4] J. Zhang, Z. Xie, J. Zhang, Y. Tang, C. Song, T. Navessin, Z. Shi, D. Song, H. Wang, and *et al.*, J. Power Sources **160**, 872 (2006).
[5] M. F. Schuster and W. H. Meyer, Annu. Rev. Mater. Res. **33**, 233 (2003).
[6] S. Y. Kim, S. Kim, and M. J. Park, Nat. Commun. **1**, 1 (2010).
[7] Y. Chen, M. Thorn, S. Christensen, C. Versek, A. Poe, R. C. Hayward, M. T. Tuominen, and S. Thayumanavan, Nat. Chem. **2**, 503 (2010).
[8] L. Vilčiauskas, M. E. Tuckerman, G. Bester, S. J. Paddison, and K.-D. Kreuer, Nat. Chem. **4**, 461 (2012).
[9] W. L. Wang and E. Kaxiras, New J. Phys. **12**, 125012 (2010).
[10] See Supplemental Material at URL, which includes Refs. [11-17], for further details.
[11] S. Nosé, J. Chem. Phys. **81**, 511 (1984).
[12] G. Kresse and D. Joubert, Phys. Rev. B **59**, 1758 (1999).
[13] K. Laasonen, A. Pasquarello, R. Car, C. Lee, and D. Vanderbilt, Phys. Rev. B **47**, 10142 (1993).
[14] J. P. Perdew, J. A. Chevary, S. H. Vosko, K. A. Jackson, M. R. Pederson, D. J. Singh, and C. Fiolhais, Phys. Rev. B **46**, 6671 (1992).
[15] J. P. Perdew, J. A. Chevary, S. H. Vosko, K. A. Jackson, M. R. Pederson, D. J. Singh, and C. Fiolhais, Phys. Rev. B **48**, 4978 (1993).
[16] P. Vassilev, C. Hartnig, M. T. M. Koper, F. Frechard, and R. A. van Santen, J. Chem. Phys. **115**, 9815 (2001).
[17] N. G. Limas and T. A. Manz, RSC Adv. **6**, 45727 (2016).
[18] G. Kresse and J. Furthmüller, Phys. Rev. B **54**, 11169 (1996).
[19] P. Giannozzi, S. Baroni, N. Bonini, M. Calandra, R. Car, C. Cavazzoni, D. Ceresoli, G. L. Chiarotti, M. Cococcioni, I. Dabo, and *et al.*, J. Phys.: Condens. Matter **21**, 395502 (2009).
[20] J. P. Perdew, K. Burke, and M. Ernzerhof, Phys. Rev. Lett. **77**, 3865 (1996).
[21] G. Henkelman, B. P. Uberuaga, and H. Jónsson, J. Chem. Phys. **113**, 9901 (2000).
[22] T. J. F. Day, A. V. Soudackov, M. Čuma, U. W. Schmitt, and G. A. Voth, J. Chem. Phys. **117**, 5839 (2002).
[23] S. Feng and G. A. Voth, J. Phys. Chem. B **115**, 5903 (2011).
[24] S. Ochi, O. Kamishima, J. Mizusaki, and J. Kawamura, Solid State Ionics **180**, 580 (2009).
[25] M. Cappadonia, J. W. Erning, S. M. S. Niaki, and U. Stimming, Solid State Ionics **77**, 65 (1995).
[26] T. Vegge, Phys. Rev. B **70**, 035412 (2004).
[27] J. T. Fermann and S. Auerbach, J. Chem. Phys. **112**, 6787 (2000).
[28] T. A. Manz and N. G. Limas, RSC Adv. **6**, 47771 (2016).
[29] G. Makov and M. C. Payne, Phys. Rev. B **51**, 4014 (1995).
[30] I. Dabo, B. Kozinsky, N. E. Singh-Miller, and N. Marzari, Phys. Rev. B **77**, 115139 (2008).
[31] A. Striolo, Nano Lett. **6**, 633 (2006).
[32] N. E. R. Zimmermann, T. J. Zabel, and F. J. Keil, J. Phys. Chem. C **117**, 7384 (2013).
[33] A. Phan, D. R. Cole, R. G. Weiß, J. Dzubiella, and A. Striolo, ACS Nano **10**, 7646 (2016).
[34] N. Agmon, Chem. Phys. Lett. **244**, 456 (1995).
[35] C. Dellago and G. Hummer, Phys. Rev. Lett. **97**, 245901 (2006).
[36] T. C. Berkelbach, H.-S. Lee, and M. E. Tuckerman, Phys. Rev. Lett. **103**, 238302 (2009).
[37] C. Dellago, M. M. Naor, and G. Hummer, Phys. Rev. Lett. **90**, 105902 (2003).
[38] C. Nagamani, U. Viswanathan, C. Versek, M. T. Tuominen, S. M. Auerbach, and S. Thayumanavan, Chem. Commun. **47**, 6638 (2011).
[39] A. Baranov, B. Merinov, A. Tregubchenko, V. Khiznichenko, L. Shuvalov, and N. Schagina, Solid State Ionics **36**, 279 (1989).
[40] V. I. Ivanov-Omskii and S. G. Yastrebov, Semiconductors **39**, 941 (2005).
[41] E. S. Kryachko and V. P. Sokhan, Proc. R. Soc. A **439**, 211 (1992).
[42] M. Baraket, S. G. Walton, E. H. Lock, J. T. Robinson, and F. K. Perkins, Appl. Phys. Lett. **96**, 231501 (2010).